Journal of
Manufacturing and Materials Processing

MDPI

Article

Development and Characterization of Stable Polymer Formulations for Manufacturing Magnetic Composites

Balakrishnan Nagarajan [1], Milad Kamkar [2], Martin A.W. Schoen [3], Uttandaraman Sundararaj [2], Simon Trudel [3], Ahmed Jawad Qureshi [1] and Pierre Mertiny [1,*]

1 Department of Mechanical Engineering, University of Alberta, 9211-116 St. NW, Edmonton, AB T6G 1H9, Canada; bnagaraj@ualberta.ca (B.N.); ajquresh@ualberta.ca (A.J.Q.)
2 Department of Chemical and Petroleum Engineering, University of Calgary, 2500 University Dr. NW, Calgary, AB T2N 1N4, Canada; milad.kamkar1@ucalgary.ca (M.K.); ut@ucalgary.ca (U.S.)
3 Department of Chemistry, University of Calgary, 2500 University Dr. NW, Calgary, AB T2N 1N4, Canada; martin.schon@ucalgary.ca (M.A.W.S.); trudels@ucalgary.ca (S.T.)
* Correspondence: pmertiny@ualberta.ca

Received: 20 December 2019; Accepted: 9 January 2020; Published: 12 January 2020

Abstract: Polymer bonded permanent magnets find significant applications in a multitude of electrical and electronic devices. In this study, magnetic particle-loaded epoxy resin formulations were developed for in-situ polymerization and material jetting based additive manufacturing processes. Fundamental material and process issues like particle settling at room temperature and elevated temperature curing, rheology control and geometric stability of the magnetic polymer during the thermal curing process are addressed. Control of particle settling, modifications in rheological behavior and geometric stability were accomplished using an additive that enabled the modification of the formulation behavior at different process conditions. The magnetic particle size and additive loading were found to influence the rheological properties significantly. The synergistic effect of the additive enabled the developing of composites with engineered magnetic filler loading. Morphological characterization using scanning electron microscopy revealed a homogenous particle distribution in composites. It was observed that the influence of temperature was profound on the coercive field and remanent magnetization of the magnetic composites. The characterization of magnetic polymers and composites using rheometry, scanning electron microscopy, X-ray diffraction and superconducting quantum interference device (SQUID) magnetometry analysis enabled the correlating of the behavior observed in different stages of the manufacturing processes. Furthermore, this fundamental research facilitates a pathway to construct robust materials and processes to develop magnetic composites with engineered properties.

Keywords: material jetting; magnetic composites; polymer formulation; particle settling; material behavior control; magnetic characterization

1. Introduction

Permanent magnets are used in a wide range of consumer and industrial applications that involve the conversion of mechanical energy to electrical energy, and vice versa. Permanent magnets find applications in areas like factory automation, medical devices, household appliances, consumer electronics and automotive systems. Permanent magnets are utilized in electro-mechanical devices such as microwave generators, motors, dynamos, actuators, speakers and magnetic couplings [1,2]. Among many permanent magnet materials, alnico, ferrites, samarium cobalt, and neodymium iron boron ($Nd_2Fe_{14}B$, abbreviated herein as NdFeB) are predominantly used in the industry. The hard-magnetic

properties of these materials make them attractive for selective applications over other magnetic material options. A permanent magnet where the magnetic powder is mixed with a polymeric binder is called a bonded magnet. Commonly utilized magnetic powders include the aforementioned magnetic materials and hybrid mixtures thereof. The binders include polyamide (PA), polytetrafluoroethylene, epoxies, polyester and polyphenylene sulphide. Four traditional processes utilized to manufacture bonded magnets are extrusion, compression molding, injection molding and calendaring [3]. The properties of the polymer bonded magnets depend on the type of magnetic filler used, the polymer binder and the distribution of the filler [4].

Magnetic composites with magnetically hard and soft fillers find applications in electrical machines due to their favorable mechanical, magnetic and physical properties. Electric motors are devices utilized to convert electrical energy to mechanical energy with high conversion efficiency [5]. One such application is a flywheel energy storage system (FESS), which utilizes an electrical machine that functions both as a motor and generator [6]. Edwards et al. developed fiber-reinforced polymer composite laminates with both mechanical and magnetic functionality for use in electromechanical applications [7]. Mechanically stiff magnetic composites with high tensile elasticity and electrical resistivity were developed using bidisperse iron particles for flywheel lift magnet applications [8]. With the motive of developing anisotropic magnetic polymer composites with enhanced magnetic characteristics, particle structuring using uniaxial and biaxial fields has been adopted to fabricate composites with chain and sheet like particle structures, respectively. To prevent the sedimentation of magnetic particles during fabrication, a magnetic field supplied by permanent magnets during the room temperature gelling of resin combined with a multistage curing methodology was utilized [9].

Additive manufacturing (AM) is a rapid prototyping technique where parts are constructed by adding materials in layers, where each layer of the part is a thin cross-section derived from a computer-aided design (CAD) file. AM enables the production of complex three-dimensional (3D) objects directly from CAD data without having to consider tooling [10]. AM of magnetic components has been an extensive field of research to develop components for the electrical and electronic industry. Researchers have studied both metal and polymer-based AM systems to manufacture magnetic functional materials. Mikler et al. demonstrated laser additive processing of three soft magnetic alloys using direct energy deposition [11]. Nilsen et al. utilized powder bed fusion to develop ferromagnetic nickel–manganese–gallium alloy and studied the influence of process parameters using structured experimental design [12]. A commercial multi-extruder 3D printer was utilized by Yan et al. for fabricating magnetic components in an effort to simplify integration processes in power electronic circuits [13]. The feasibility of AM processes to fabricate complex magnetic components by printing a conductive winding along with a magnetic core has been reported in the technical literature [14]. Additionally, improvements in magnetic properties were reported by adjusting the feed paste formulation, its flow characteristics and AM process parameters. Direct-write AM of NdFeB polymer bonded permanent magnets using epoxy as a binder was demonstrated by Compton et al. [15]. In other research, big area additive manufacturing of isotropic NdFeB powder in PA binder enabled the manufacturing of magnets with enhanced remanence and coercive field compared to traditional injection-molded magnets [16]. Polymer bonded permanent magnets with anisotropic properties were developed by applying an external magnetic field with intensities varying from 5 kOe to 50 kOe using an electromagnet as a part of the post printing process [17]. Methodologies to orient ferromagnetic particles at user defined angles and the influence of external magnetic field strength on degree of particle alignment at lower filler loadings for AM process have been reported in the technical literature [18]. Magnetic products based on strontium ferrite ($SrFe_{12}O_{19}$, abbreviated herein as SrFeO) and NdFeB were fabricated using the extrusion of developed strips and filaments using ethylene ethyl acrylate as a binder [19]. Stainless steel microparticles in an acrylonitrile butadiene styrene polymer matrix were 3D printed with the motive of utilizing the resulting parts in the application of passive magnetic sensors and actuators [20]. Magnetic composites using a NdFeB/PA magnetic filament were printed for the prototype of a rotary blood pump and successfully integrated [21]. Research related to 3D

printing polymer bonded magnets has mainly been focused on thermoplastic polymers and enhancing magnetic filler loading and efficiency. Thermoplastic filaments with engineered magnetic particle content for AM have already been reported in the technical literature [20]. In contrast, developing a methodology to engineer magnetic particle content in 3D printed thermoset composites has received limited attention and is thus one of the many challenges addressed in the present work.

In this research, the authors develop and engineer magnetic pastes for in-situ polymerization and material jetting-based AM processes. First, magnetic pastes were engineered to prevent particle settling at room temperature and at elevated curing temperatures. X-ray diffraction (XRD) analysis was utilized to validate the ability of the material formulations to resist gravitational particle settling after the thermal curing process. The rheological properties of the magnetic pastes with multi modal magnetic particles and an additive material were characterized. These results were utilized to elucidate the material behavior encountered in different stages of the manufacturing process. Developed magnetic pastes were further used to print 3D magnetic structures using an in-house developed material jetting 3D printer. Tailoring the paste rheology enabled the printing of magnetic composites with engineered magnetic particle loading without significant deformation after the curing process. The particle distribution in 3D printed magnetic composites was characterized using scanning electron microscopy (SEM). Magnetic characterization of 3D-printed composites was conducted using a SQUID (superconducting quantum interference device) magnetometer. The results from this research enable an in-depth understanding of the role that engineered material formulations play in overcoming several manufacturing process issues and demonstrate the clear benefits of utilizing tailored rheology to one's advantage.

2. Materials and Methods

For this study, anisotropic NdFeB powder (type MQA-38-14) was purchased from Magnequench Inc. (Singapore), and SrFeO powder was purchased from Dowa Electronics Materials Co. Ltd. (Tokyo, Japan). For the polymer, a bisphenol A based epoxy resin, EPON 826, with an aromatic amine curing agent, EPICURE W, were used (Hexion Inc., Columbus, OH, USA). Disparlon 6900-20X obtained from King Industries (Norwalk, CT, USA) was used as an anti-settling additive and shear thinning agent. Table 1 lists the physical properties of the magnetic particles and the epoxy resin.

Table 1. Physical properties of materials utilized (as obtained from manufacturers).

Material Type	Average Particle Size	Density [g/cm^3]
MQA-38-14 (NdFeB)	90 μm	7.51
SF-500 (SrFeO)	1.41 μm	3.41
EPON 826	-	1.16

2.1. Scanning Electron Microscopy

The morphology of the magnetic particles and the magnetic particle-reinforced composites was studied using a Zeiss Sigma 300 VP field-emission scanning electron microscope (Oberkochen, Germany) equipped with secondary and backscattered electron detectors. Prior to imaging, the composite samples were cut, polished, and finally coated with carbon using a Leica EM SCD005 evaporative carbon coater (Wetzlar, Germany) to prevent the charging of the composite surface.

2.2. Preparation of Magnetic Paste Formulations

The composite mixtures were prepared from epoxy resin, which in some cases was modified with the rheological additive, and magnetic particles by mechanical mixing using an impeller agitator from Calframo Ltd. (Georgian Bluffs, ON, Canada). The additive material was premixed with the epoxy resin to create a polymer base (additive modified epoxy is herein abbreviated as aZEPX where 'Z' indicates the additive weight fraction). For rheological studies, the magnetic particles were then

added in increments to the polymer base to meet the desired filler loading (i.e., the magnetic filler to base polymer ratio). For the 3D-printed and cured samples used in the magnetic characterization, the required quantity of the curing agent was included in the amount of base polymer when determining the mass of magnetic filler to ensure the desired filler loading was achieved. Acetone was used to aid in the dispersion process. The curing agent, when needed, was added as the last component of the magnetic paste formulation. After blending, the composite mixtures were degassed in vacuum to remove entrapped volatiles.

2.3. Rheological Characterization

The rheological behavior of magnetic paste formulations was assessed using an Anton–Parr MCR 302 rheometer equipped with a 25 mm diameter parallel plate geometry. Table 2 lists the material formulations that were characterized for their rheological properties. For all the rheological tests, the magnetic filler loading in the magnetic paste formulations was maintained at 50 wt%. Hy-EPX sample, which is a hybrid formulation, containing 30 wt% of NdFeB and 20 wt% of SrFeO.

Table 2. Materials characterized for rheological properties.

Sample Name	Material Type	Magnetic Filler Loading
EPX	Pure epoxy	-
NdFeB-EPX	NdFeB + epoxy	50 wt%
SrFeO-EPX	SrFeO + epoxy	50 wt%
Hy-EPX	NdFeB + SrFeO + epoxy	50 wt%
NdFeB-a5EPX	NdFeB + epoxy modified with 5 wt% additive	50 wt%
NdFeB-a10EPX	NdFeB + epoxy modified with 10 wt% additive	50 wt%

The viscosity of the magnetic pastes was monitored as a function of shear rate at room temperature. A single rheological experiment was performed for each of the materials listed in Table 2. The resulting flow curve data were constructive for deriving a fundamental understanding of how rheological properties are influenced by magnetic particle size and additive loading. The yield stress, defined as the shear stress at zero shear rate, was estimated by curve fitting of the Herschel–Bulkley model (as shown in Equation (1)) to flow curve data.

$$\tau = \tau_0 + C\dot{\gamma}^n \quad (1)$$

Here, τ_0 is the yield stress, C is the consistency index, τ is the shear stress, $\dot{\gamma}$ is the shear rate and n is the flow index. The value of the flow index enabled the classification of material behavior as shear thinning ($n < 1$), shear thickening ($n > 1$), or Bingham fluid ($n = 1$) [22]. The shear thinning index (STI)—the ratio of viscosity at two different shear rates—was used to estimate the extent of non-Newtonian behavior exhibited by the magnetic paste formulations [23]. Rheological analysis of magnetic pastes is essential for understanding the paste behavior at different shear rates experienced by the paste inside the cylinder barrel and nozzle for 3D printing processes [24]. Moreover, to understand the influence of temperature on flow behavior, the viscosity of the magnetic pastes was measured at different temperatures (i.e. 60, 80 and 100 °C) with increasing shear rates. The Arrhenius equation is widely used to describe the relationship between viscosity and temperature, i.e.,

$$\eta = A \cdot e^{E_\eta / RT} \quad (2)$$

where E_η is the flow activation energy, R is the ideal gas constant, T is the absolute temperature, A is the regression coefficient and η is viscosity [25,26].

Oscillatory rheology measurements (e.g., frequency sweep tests) were also conducted on the magnetic pastes to determine the viscoelastic properties, such as storage modulus (G′), loss modulus (G″) and damping factor (tan δ) of the samples. Studying the viscoelastic response of the samples provided the opportunity of identifying whether the magnetic pastes exhibited liquid like or solid like

behavior, which enabled the evaluation of the effects of the particulate microstructure in the polymeric matrix. Frequency sweep tests have previously been utilized to evaluate the material consistency at rest, storage stability, sedimentation, synergies and phase separation of polymeric dispersions [22].

2.4. Particle Settling Evaluation in Uncured and Cured Magnetic Polymer Composites

The capability of the rheological additive to mitigate particle settling at room temperature was assessed using simple sedimentation experiments, where particle settling effects were captured using digital photographs. The magnetic paste formulations listed in Table 2 were utilized for the experiments. The prepared pastes were transferred into transparent glass beakers where settling assessment experiments were conducted. To evaluate the capability of the material formulation to withstand particle settling at elevated curing temperatures, a measured quantity of the magnetic paste formulation was transferred to a small aluminum cuvette and subsequently cured in an oven at 80 °C for 4 hours. Additionally, particle settling was evaluated using XRD tests. XRD measurements were performed using a Geigerflex 2173 diffractometer (Rigaku Corporation, Tokyo, Japan) fitted with a Co-tube X-ray source (λ = 1.789 Å; 38 kV and 38 mA) and a graphite monochromator to filter the Co K-β wavelength. The samples were scanned over 2θ, ranging from 30° to 90° at a rate of 2 °/min. Both the top and bottom surface of the cured samples were analyzed. The cured samples were also analyzed over their cross-section via SEM to corroborate findings derived from XRD testing.

2.5. Additive Manufacturing of Magnetic Polymer Composites

A material jetting-based additive manufacturing technique was utilized to deposit the magnetic pastes and fabricate the magnetic composites. For this purpose, an in-house developed material jetting platform was equipped with a precision dispensing system (Ultimus V, Nordson EFD, East Providence, RI, USA), controlled using the Labview software environment [27] (National Instruments, Austin, TX, USA). A graphical user interface enabled the adjusting of the dispensing pressure and deposition speed. The open source software Sli3cr was used to generate the g-code for the tool path based on given input parameters like layer thickness, extruded material width and infill pattern [28]. Deposition trials were conducted to determine the feasible parameter combinations prior to actual composite fabrication.

2.6. Magnetic Characterization

The materials listed in Table 3 were mixed, 3D printed, cured and then used for magnetic characterization. The target magnetic filler loading was 80 wt% for NdFeB80-a10EPX-C, SrFeO80-a10EPX-C and Hy80-a10EPX-C, and 50 wt% for NdFeB-a10EPX-C, with the base polymer for all samples comprising 10 wt% rheological additive ('C' in the material identifier indicates cured epoxy pastes). Small pieces from the 3Dprinted, not pre-magnetized samples were weighed and then placed in gelatin capsules, which were themselves inserted into clear and diamagnetic plastic straws.

Table 3. Materials 3D printed and characterized for magnetic properties.

Material Number	Material Type	Magnetic Filler Loading
NdFeB80-a10EPX-C	NdFeB + epoxy modified with 10 wt% additive	80.2 wt%
SrFeO80-a10EPX-C	SrFeO + epoxy modified with 10 wt% additive	80.1 wt%
Hy80-a10EPX-C	NdFeB + SrFeO + epoxy modified with 10 wt% additive	80.8 wt%
NdFeB-a10EPX-C	NdFeB + epoxy modified with 10 wt% additive	50.1 wt%

The magnetic properties of the polymer composites were measured using a SQUID magnetometer (MPMS XL-7 Evercool, Quantum Design, San Diego, CA, USA). Magnetization reversal loops were measured for each composite listed in Table 3 in magnetic field strengths of $\mu_0 H = \pm 7$ T at temperatures of 325, 350, 375 and 395 K. The saturation magnetization was determined at a field of 7 T. The remanence and coercivity were quantified by the linear interpolation of the magnetization at zero applied field,

and the applied field at zero magnetization, respectively. The magnetic parameters were determined by averaging the values for both field sweep directions.

3. Results

3.1. SEM Characterization of Magnetic Fillers

Figure 1 shows the morphological features of magnetic particles investigated via SEM. The images of NdFeB and SrFeO particles indicate irregular morphology. Even though particle size data was obtained from material data sheets, particles dimensions were measured in the SEM images using the ImageJ software (National Institutes of Health, Bethesda, MD, USA) [29]. Particle linear dimensions ranging from 5 to 120 µm were observed for anisotropic NdFeB, and 0.5 to 5 µm for anisotropic SrFeO, indicating a wide particle size distribution of the magnetic fillers. It is assumed that smaller particles enabled the enhancing of the loading fraction by filling in gaps between larger particles.

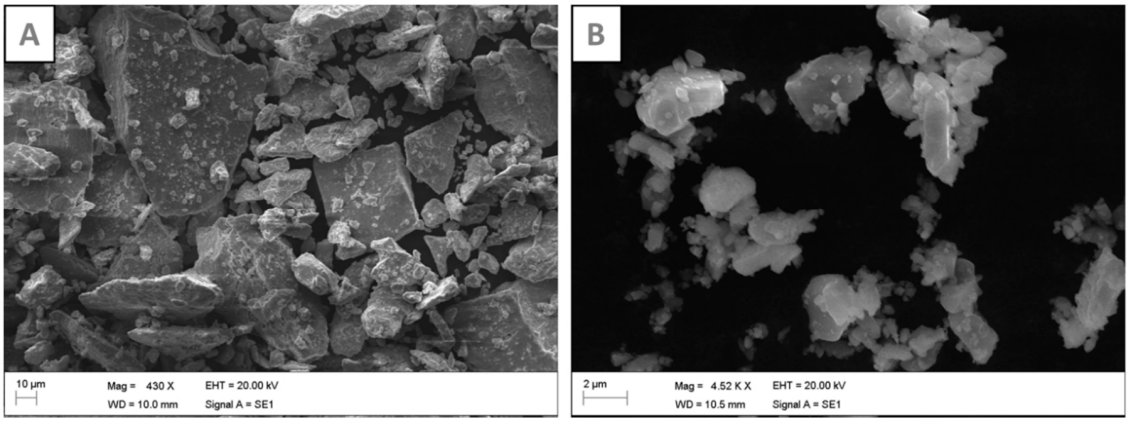

Figure 1. SEM images of magnetic particles: (**A**) NdFeB and (**B**) SrFeO.

3.2. Rheological Analysis of Magnetic Pastes

3.2.1. Viscosity and Flow Curve Analysis

Rheological properties of magnetic pastes play a significant role in controlling and optimizing the manufacturing process conditions. The rheological behavior of complex material systems depends on a multitude of parameters, including particle size, shape, filler volume fraction, inter-particle and filler-matrix interactions [30]. The rheological properties of the samples under rotational and oscillatory flow fields were analyzed to study the effects of particle size and rheological additive on flow behavior and network structure of the magnetic pastes.

Apart from the pure epoxy that exhibits a Newtonian flow behavior (shear rate independent), all magnetic pastes exhibit non-Newtonian behavior, which can be identified by a decrease in the viscosity of the magnetic pastes with increasing shear rate (see Figure 2). Utilizing Equation (1), the rheological properties of the magnetic pastes (i.e., yield strength, flow index and consistency index, listed in Table 4) were derived in order to investigate the influence of the constituent materials utilized to formulate the magnetic pastes. In general, for all the magnetic paste formulations, the flow index, which represents the degree of pseudo-plasticity, was found to be less than unity (i.e., $n < 1$), indicating shear thinning behavior. Additionally, STI values greater than unity confirm pseudo-plastic behavior, and the magnitude of the STI values for all the magnetic pastes enabled us to understand the extent of pseudo-plasticity within the probed range of shear rate window. It was observed that fine SrFeO particles and rheological additives significantly enhanced the yield strength of the magnetic paste formulations. To elaborate on this observation, NdFeB-EPX sample, compared to SrFeO-EPX sample, exhibits lower viscosity at low shear rates (see Figure 2), which is attributed to the higher surface area to volume ratio of SrFeO as compared to NdFeB. Hence, for the same filler loading in the magnetic

pastes, SrFeO particles feature a considerably greater surface area compared to NdFeB. The effect of fine SrFeO particles is clearly observed in the yield strength of the magnetic pastes, which is 30 times higher than that of samples containing NdFeB particles. The hybrid magnetic paste (Hy-EPX) exhibited significant enhancement in low-shear viscosity and yield strength compared to NdFeB-EPX sample. Again, this enhancement is attributed primarily to the presence of fine SrFeO particles. A decrease in flow index for materials SrFeO-EPX and Hy-EPX compared to NdFeB-EPX is congruent to findings in the technical literature, where a reduction in flow index was observed with decreasing particle size [26].

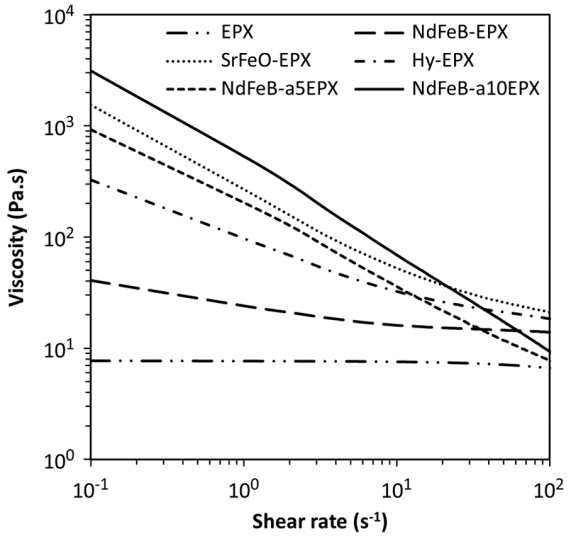

Figure 2. Viscosity as a function of shear rate for the magnetic pastes as listed in Table 2.

Table 4. Derived rheological properties of the magnetic pastes as listed in Table 2.

Material Number	Yield Strength [Pa]	Flow Index-*n*	Consistency Index-*C*	STI
EPX	-	-	-	1
NdFeB-EPX	7.87	0.96	17.02	3
SrFeO-EPX	235.16	0.82	43.48	30
Hy-EPX	67.77	0.84	36.92	10
NdFeB-a5EPX	159.40	0.49	63.24	26
NdFeB-a10EPX	232.66	0.19	302.37	46

Referring to Figure 2 and Table 4, comparing sample NdFeB-EPX with NdFeB-a5EPX and NdFeB-a10EPX reveals that the addition of the rheological additive (Disparlon 6900-20X) significantly increased the low shear viscosity and yield strength of the magnetic pastes. This rheological additive is known to create a 3D network through hydrogen bonding with epoxy polymer chains resulting in a gel-like structure. Epoxy resins containing the rheological additive exhibit shear thinning behavior through the disruption of the network structure, while the formation of hydrogen bonds imparts thixotropic properties, enabling time-dependent changes in viscosity [31]. Comparing flow behavior of samples NdFeB-a5EPX and NdFeB-a10EPX, it can be concluded that an increase in rheological additive content fostered strong shear thinning behavior, which is supported by a low flow index value. Overall, the addition of fine SrFeO particles and the rheological additive raised the yield strength compared to samples containing only NdFeB particles, which is highly desirable for the considered 3D printing processes.

3.2.2. Influence of Temperature on Viscosity

The temperature dependence of viscosity must be carefully considered to control particle settling at elevated curing temperature in in-situ polymerization and to ensure geometric stability in material

jetting processes. As is observed in Figure 3A, the viscosity of all the magnetic paste formulations decreased with increasing temperature. It is clearly observed that rheological additives in samples NdFeB-a5EPX and NdFeB-a10EPX enabled maintaining higher shear viscosity up to 100 °C compared to formulations without an additive.

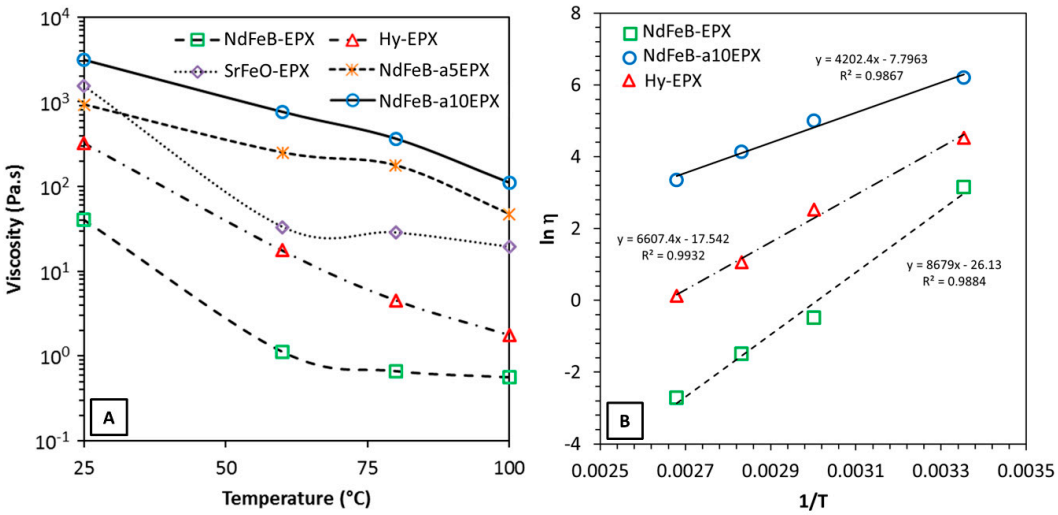

Figure 3. (**A**) Viscosity as a function of temperature at shear rate of 1 s^{-1} for magnetic paste materials listed in Table 2. (**B**) Viscosity–temperature data linear curve fitting with linearized Arrhenius equation (Equation (2)) for NdFeB based magnetic paste materials NdFeB-EPX, Hy-EPX and NdFeB-a10EPX (as per Table 2).

The observed material behavior is consistent with the Arrhenius law presented in Equation (2) where viscosity has a negative correlation with temperature. Modifying Equation (2), it can be shown that ln(η) has a linear relationship with 1/T. For example, the magnetic pastes containing NdFeB (samples NdFeB-EPX, Hy-EPX and NdFeB-a10EPX) exhibit such a linear relation with good agreement, as indicated by Figure 3B. It can be observed that the rate of viscosity decrease is substantially lower for the formulation engineered with the rheological additive (NdFeB-a10EPX) as compared to the other NdFeB composites (NdFeB-EPX and Hy-EPX), confirming that formulations engineered with the rheological additive are less susceptible to temperature changes. Furthermore, the activation energy was calculated from the slope of ln (η)–(1/T) curves with the known R value according to Equation (2). The activation energies (E_η) obtained for NdFeB-EPX, Hy-EPX and NdFeB-a10EPX are 72.2 kJ/mol, 54.9 kJ/mol and 34.9 kJ/mol, respectively. It is observed that the formulation engineered with rheological additive (NdFeB-a10EPX) exhibited a lower activation energy compared to the formulation without additive (NdFeB-EPX). Activation energy is an indicator used to characterize the thermal susceptibility of materials. Materials with low activation energy were observed to be less susceptible to temperature changes [26,32]. Additionally, the chosen rheological additive (Disparlon 6900-20x) is PA based with a high melting point, which extends its activity to high temperature ranges [33].

3.2.3. Oscillatory Rheology Analysis of Magnetic Paste Formulations

Oscillatory frequency sweeps have been widely used to characterize polymer filled samples (polymer composites, polymer solutions, etc.) [34,35]. Information about a sample's rigidity and network structure can be obtained by studying viscoelastic parameters, such as the storage modulus (G'), loss modulus (G'') and damping factor (tan δ) [36]. The storage and loss moduli are indicative of the energy that is stored and dissipated in the material, respectively. In the present study, the viscoelastic characteristics of the pastes were probed using frequency sweep tests conducted over an angular frequency (ω) ranging from 0.1 to 100 rad/s at a constant shear strain γ_0 = 1%. Figure 4A,B depict the frequency dependence of G' and G'' on ω, respectively. For samples NdFeB-EPX, SrFeO-EPX

and Hy-EPX, the loss modulus was greater than the storage modulus ($G'' > G'$) for the entire range of probed frequencies, which indicates that the viscous character is dominant. For samples NdFeB-a5EPX and NdFeB-a10EPX, which contain the rheological additive, the opposite behavior was observed, i.e., the storage modulus was higher than the loss modulus ($G' > G''$), signaling a solid-like behavior. This change in the material behavior is imparted by the rheological additive due to the formation of a gel character via hydrogen bonding. Moreover, it is observed that the gradient in modulus curves over the frequency range for magnetic pastes with the rheological additive is considerably less than for the pastes without additive. This characteristic indicates reduced material flowability, which further corroborates the existence of gel-like behavior in pastes containing the rheological additive. Given the observations made for the storage and loss moduli, the ratio of loss modulus to storage modulus ($\tan \delta = G''/G'$) is less than unity for magnetic paste formulations containing the rheological additive (NdFeB-a5EPX and NdFeB-a10EPX) whereas $\tan \delta > 1$ for the other paste formulations. As such, the findings are congruent with the notion that higher $\tan \delta$ values are indicative of greater energy dissipation, as in the case of the magnetic paste formulations without rheological additive. Hence, oscillatory and rotational rheometry confirm that the used additive confers the vital prerequisites for 3D printing of the magnetic pastes.

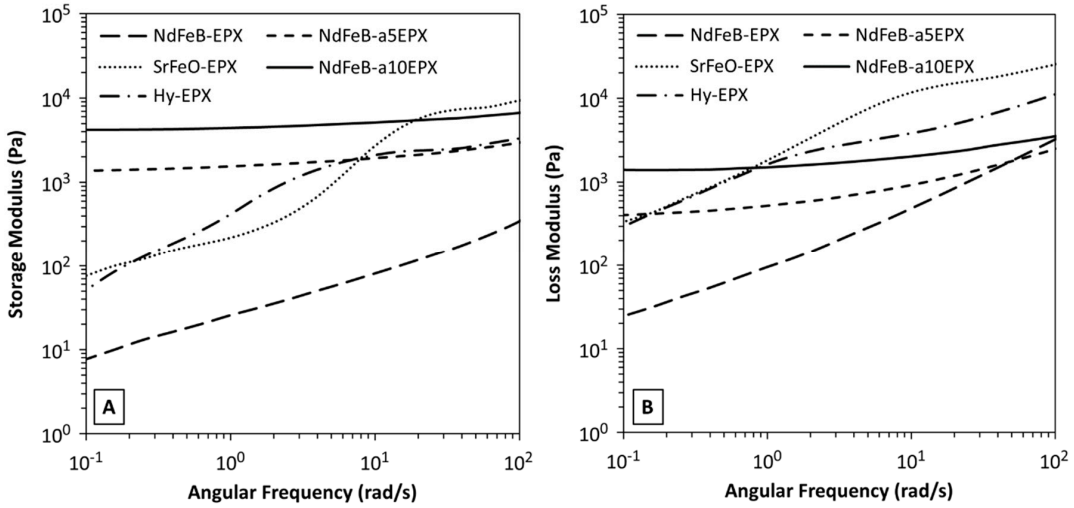

Figure 4. (**A**) Storage modulus G' and (**B**) loss modulus G'' as a function of angular frequency for magnetic paste materials listed in Table 2.

3.3. Analysis of Magnetic Particle Settling in Uncured Resin and Cured Polymer Composites

3.3.1. Particle Settling at Stationary Conditions

Magnetic particle settling in polymers is primarily due to gravity and affects the stability of the paste formulation. In the case of material jetting processes, where paste deposition through a nozzle is driven by pressure, additional inertia is exerted on particles, typically in the downward direction, which may further intensify particles' settling effects. Moreover, particle settling may lead to the clogging of the nozzle and thus create a disruption in the manufacturing process. In this study, the means to address particle settling was adding the rheological additive to the magnetic paste formulations. Figure 5 shows the ability of the rheological additive to mitigate gravitational particle settling. Eight hours after filling the beaker, filler sedimentation and a clear supernatant is visible for material NdFeB-EPX, while NdFeB-a5EPX and NdFeB-a10EPX are still uniformly mixed, exhibiting an anti-settling characteristic. The rheological tests indicated that the additive causes a gelling effect in the magnetic paste formulations, presumably due to the development of a thixotropic network structure. Hence, the rheological additive, providing high viscosity at low shear rates, high yield

strength, and a greater storage modulus, effectively mitigated particle settling and promoted a stable paste formulation in stationary conditions.

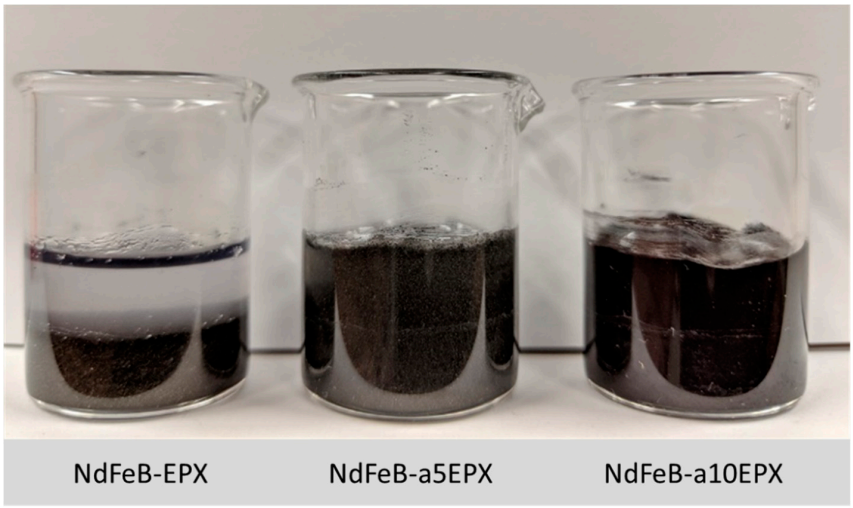

Figure 5. Photograph of clear supernatant in material NdFeB-EPX, while NdFeB-a5EPX and NdFeB-a10EPX exhibit an anti-settling characteristic.

3.3.2. Particle Settling in Cured Magnetic Polymer Composites—In-Situ Polymerization

Magnetic particle settling during the thermal curing process was investigated in samples manufactured using in situ polymerization, where the magnetic paste was transferred to a cuvette and cured at 80 °C. Paste formulations NdFeB-a5EPX and NdFeB-a10EPX were utilized in this set of experiments. The top and bottom surfaces of the cured samples were examined via XRD (see Figure 6). Strong XRD peaks of crystalline NdFeB were obtained from the bottom surfaces of the samples fabricated using both NdFeB-a5EPX and NdFeB-a10EPX, suggesting the presence of near-surface NdFeB particles (Figure 6B). Similarly, the top surface of the sample fabricated from NdFeB-a10EPX also exhibited strong crystalline peaks (Figure 6A). In contrast, the amorphous polymer peak dominants for the top surface of the NdFeB-a5EPX sample with other peaks having markedly reduced intensity, which suggests that near-surface NdFeB particles are largely absent due to settling. The XRD results thus reflect the effectiveness of the rheological additive to mitigate particle settling during the thermal curing process.

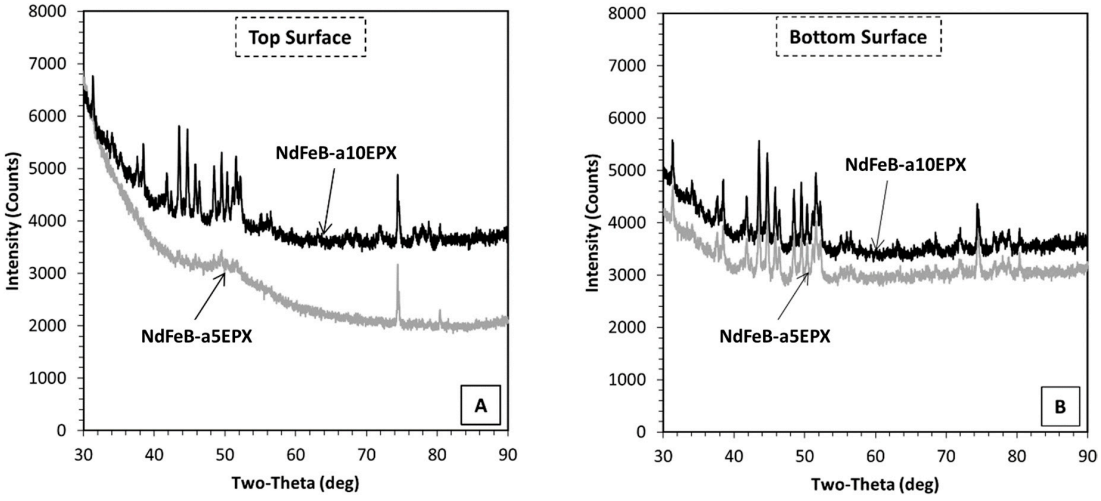

Figure 6. XRD diffractograms from (**A**) top surface (**B**) bottom surface of cured materials NdFeB-a5EPX and NdFeB-a10EPX (as per Table 2).

Cross-sections of the cured samples were further studied via SEM to validate the suppositions derived from the XRD study. In Figure 7, the sample fabricated using material NdFeB-a5EPX features a polymer-rich layer devoid of particles with an approximate thickness of 200 µm; in the sample made from NdFeB-a10EPX, particles are visible at and near the sample surface. It thus appears that some particle settling occurred in the material NdFeB-a5EPX sample, causing the observed suppression of XRD peaks.

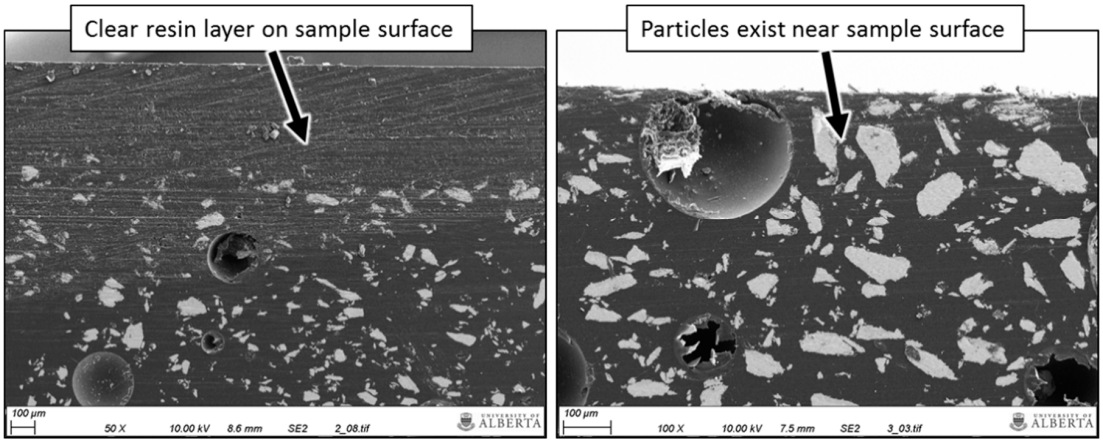

Figure 7. SEM cross-section images illustrating reduced particle settling in a sample of cured material NdFeB-a10EPX (right) compared to NdFeB-a5EPX (left) (as per Table 2). The top of the micrographs corresponds to the sample's upper surface. Some entrapped air bubbles are visible as well.

3.4. Additive Manufacturing and Characterization of Magnetic Composites

3.4.1. Geometric Stability Observations in 3D Printed Magnetic Composites

One of the fundamental goals of this work was to print magnetic composites using engineered paste formulations containing magnetic particles. Magnetically loaded polymer composites were thus fabricated from the developed paste formulations using an in-house developed material jetting 3D printer. Prior to 3D printing, trials were conducted to determine the apt printing parameters, including deposition pressure, layer thickness and deposition speed. The utilized layer thickness setting varied between 0.5 and 1.2 mm and the adopted printing speed range was between 5 and 10 mm/s. The deposition pressure for printing composites was observed to depend on the printed magnetic pastes. The formulations containing SrFeO demanded high deposition pressures, ranging from 137 to 275 kPa; for the NdFeB formulations, the required deposition pressures were between 21 and 103 kPa. In some cases, it was required to adjust the deposition pressure and layer thickness settlings during part fabrication, as adopting the same parameters for multilayer structures resulted in gaps between the deposited layers and discontinuous prints. Initially, samples were manufactured using materials NdFeB-EPX, NdFeB-a5EPX and NdFeB-a10EPX. Figure 8 shows the final shapes of the 3D-printed magnetic composites after thermal curing. It can be observed that only the paste formulations engineered using the rheological additive (NdFeB-a5EPX and NdFeB-a10EPX) retained the printed shape adequately. From rheological measurements, the formulation without the rheological additive (NdFeB-EPX) had low yield strength and exhibited viscoelastic fluid behavior, in contrast to materials NdFeB-a5EPX and NdFeB-a10EPX. The ability of the rheologically modified resin to maintain a comparatively high viscosity over a broad temperature range, especially at curing temperatures, enabled the materials to maintain the printed geometry.

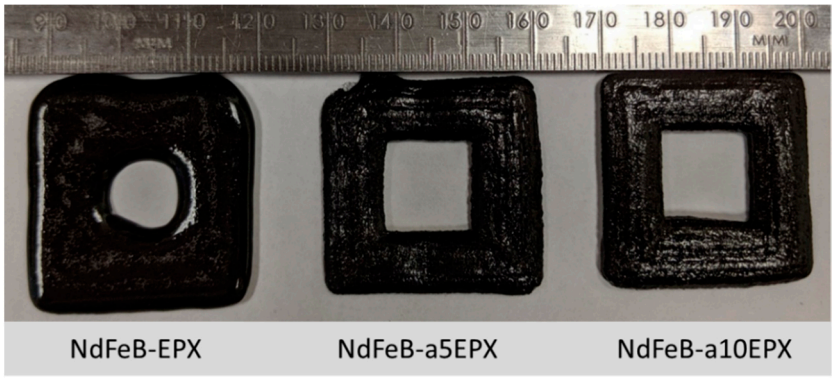

Figure 8. Geometry of 3D-printed composites (30 mm by 30 mm CAD dimensions) after thermal curing for paste formulations NdFeB-EPX, NdFeB-a5EPX and NdFeB-a10EPX (as per Table 2).

3.4.2. SEM and Magnetic Characterization of 3D Printed Composite Magnets

Using SEM and the SQUID magnetometer, composites printed using the material jetting process were characterized for their microstructure and magnetic properties (e.g., saturation magnetization, remanence and coercivity), respectively. Note that even though the deformation of the deposited pastes was adequately controlled using 5 wt% rheological additive, 10 wt% additive was employed for the analyses, as this additive loading was more effective in controlling particle settling.

The SEM images from the (cut and polished) surface of the printed magnetic composites exhibit a homogenous microstructure with well distributed particles, as seen in Figure 9. The presence of resin-rich regions in sample NdFeB80-a10EPX-C (80.2 wt% NdFeB) is an indication that the magnetic filler loading can be further enhanced to fill gaps between particles. Some porosity is also observed in the composites. The presence of porosities indicates an opportunity to improve mixing and degassing processes. Less porosity could be observed for composite SrFeO80-a10EPX-C, which features the smaller SrFeO particles. Material Hy80-a10EPX-C, which is a mixture of 60.1 wt% NdFeB and 20.7 wt% SrFeO, indicates good distribution of smaller and larger particles in the composite. Material NdFeB-a10EPX-C, which has the lower NdFeB filler loading of 50 wt%, exhibits good distribution of magnetic particles; no signs of particle agglomeration are observed. Utilizing the ImageJ software, the sizes of the NdFeB and SrFeO particles were derived from SEM images of composite samples. The measured linear dimensions of particles, expressed in the histograms in Figure 10, indicate a wide particle size distribution, as indicated by the powder manufacturers.

Permanent magnets are characterized by remanence and coercivity, i.e., their ability to supply sufficient magnetic flux, and withstand demagnetization, respectively. High values of remanence and coercivity indicate strong magnetic performance. Figure 11 shows the hysteresis data obtained for the powder and magnetic composite samples fabricated in this research. Obtained hysteresis loops were observed to be similar to the ones reported in technical literature for isotropic bonded magnets [15,37].

Figures 12 and 13 show, respectively, the saturation magnetization (M_s), remanence (M_r) and coercive field (H_c) extracted from hysteresis loops at temperatures between 300 and 400 K for the composite samples and powders. In these figures, the extracted data from the hysteresis loops are depicted with best linear fits to ease understanding the overall influence of temperature on magnetic properties. The errors are estimated to be ±5 emu/g for remanence and saturation magnetization and ±0.1 kOe for the coercive field for all samples. The values of magnetic saturation for all the composite samples match within the error band of the loading-adjusted powder saturation magnetization, which indicates that the saturation magnetization is not influenced by the composite fabrication process. Remanence for samples containing NdFeB (NdFeB80-a10EPX-C, Hy80-a10EPX-C and NdFeB-a10EPX-C) behaves similarly and follows the loading adjusted powder remanence. The composite containing only the SrFeO filler (SrFeO80-a10EPX-C), however, exhibited a decrease in remanence that exceeds the expected decrease due to the loading factor. It is thus deduced that magnetic properties not only depend on

the magnetic characteristics of the powder but are also a function of filler distribution and dispersion within the epoxy polymer. In general, the measured values of remanence are comparable with the values reported in the technical literature for NdFeB- and SrFeO-bonded magnets [19].

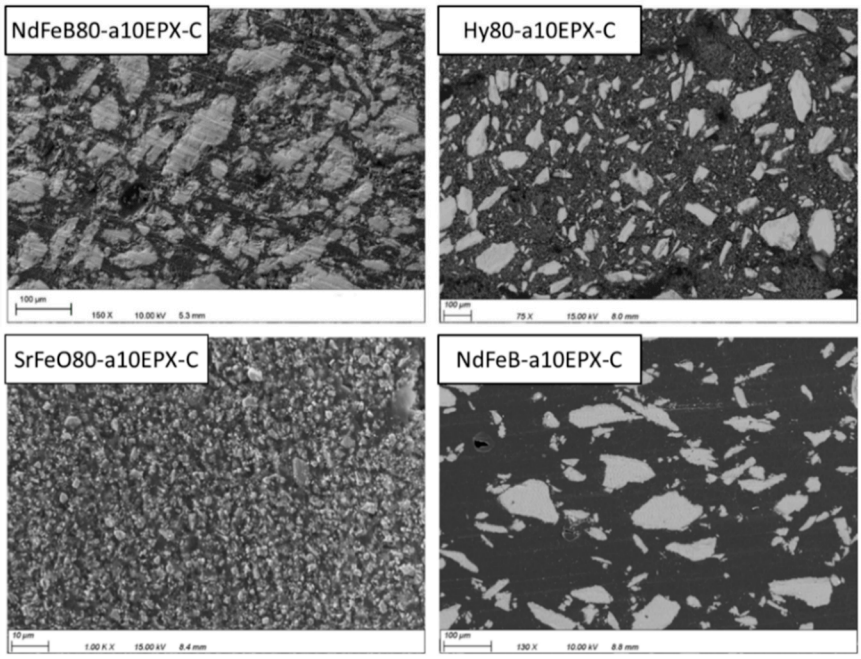

Figure 9. SEM images of magnetic composites listed in Table 3.

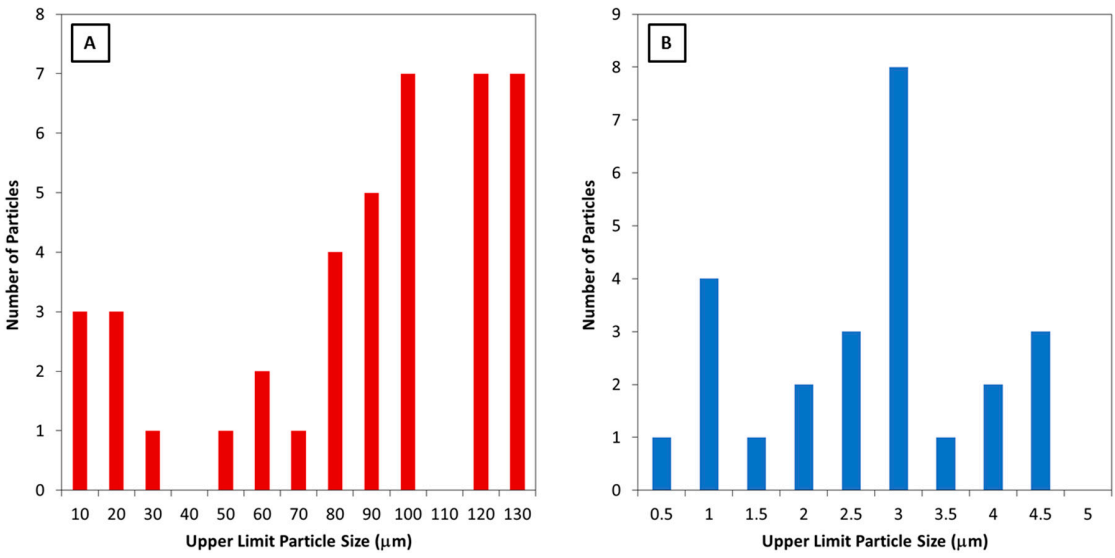

Figure 10. Size distribution of (**A**) NdFeB and (**B**) SrFeO particles in manufactured magnetic composites obtained from SEM micrographs.

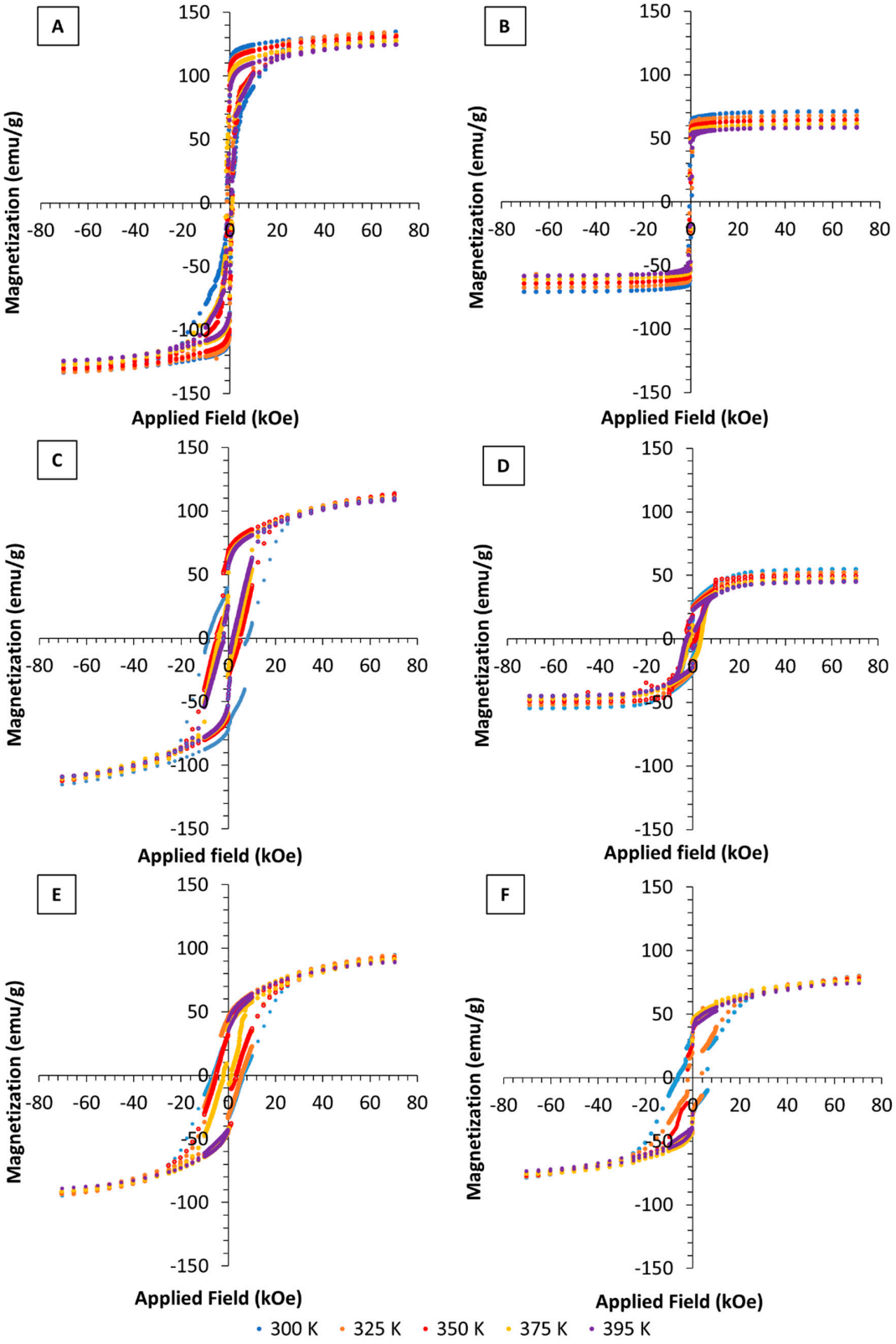

Figure 11. Hysteresis data for magnetization versus applied magnetic field, for (**A**) NdFeB powder, (**B**) SrFeO powder, cured materials: (**C**) NdFeB80-a10EPX-C, (**D**) SrFeO80-a10EPX-C, (**E**) Hy80-a10EPX-C and (**F**) NdFeB-a10EPX-C (as per Table 3).

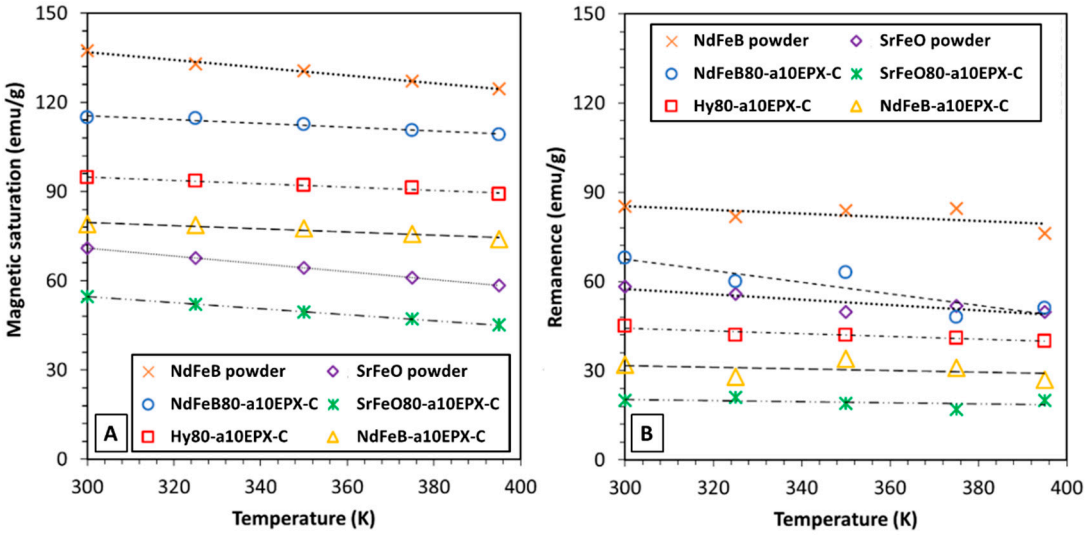

Figure 12. (**A**) Saturation magnetization and (**B**) remanence of magnetic fillers and 3D-printed magnetic composites (as per Table 3).

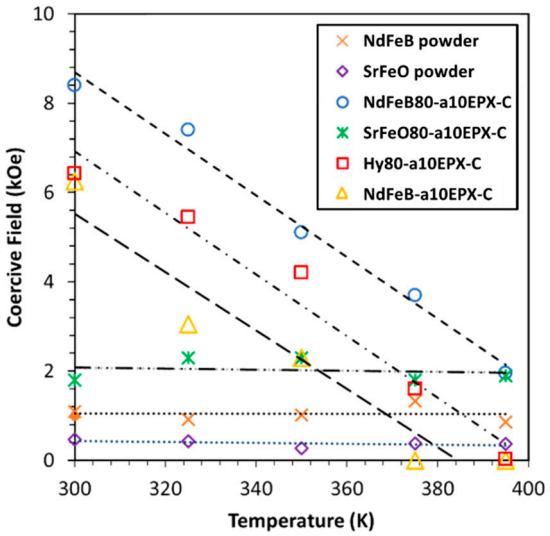

Figure 13. Coercive field of magnetic fillers and 3D-printed magnetic composites (as per Table 3).

The remanence to saturation ratio, which determines the degree of anisotropy, varies between 0.35 and 0.59 for all samples in the studied temperature range. Note that a remanence to saturation ratio greater than 0.5 indicates the transition in magnetic properties from isotropic to anisotropic [37]. It is unclear whether ratios greater than 0.5, as observed herein, are caused by interparticle interactions. In terms of temperature, an increase resulted in reductions in saturation, remanence and coercivity (see Figures 11–13). Within the given error band, composites and powders exhibited similar temperature dependencies. Note that a reduction in M_s, M_r and H_c with increasing temperature is commonly observed in magnetic materials. Notably, material SrFeO80-a10EPX-C was the most stable of the magnetic composites over the temperature range, which is consistent with the properties of the powder. It was observed that material NdFeB80-a10EPX-C exhibited a stronger dependence on temperature with respect to magnetic saturation and remanence compared to all other materials. It is noted from the technical literature that the NdFeB phase undergoes spin reorientations due to the temperature dependence of anisotropy [38]. In general, magnetic filler loading is observed to influence the coercive field. Material NdFeB-a10EPX-C (50.1 wt% magnetic filler) exhibited lower coercivity compared to NdFeB80-a10EPX-C (80.2 wt% magnetic filler). Overall, the latter magnetic

composite (NdFeB80-a10EPX-C) exhibited the best magnetic characteristics among the tested material formulations. Notably, the coercive field of NdFeB80-a10EPX-C at room temperature exceeds the properties of injection molded magnets from the same powder as mentioned in technical data sheets. No benefits in terms of M_s and M_r could be ascertained by mixing SrFeO with NdFeB powders (Hy80-a10EPX-C), as this material behaved as expected from a simple mass weighted addition of constituents' properties. This extends to the behavior for H_c, where the addition of SrFeO did not achieve an increase at high temperatures. These findings are consistent with other research [39].

4. Conclusions

In this study, stable magnetic powder-based material formulations were developed and tested that can be utilized for in situ polymerization and material jetting-based additive manufacturing processes. It was observed that the addition of a rheological additive into epoxy enhanced the desired rheological properties, i.e., viscosity at low shear rates, yield strength, degree of shear thinning and storage modulus of the magnetic paste formulation. A transition in the material behavior from viscoelastic fluid to viscoelastic solid was observed in formulations that contained the rheological additive. The material modified with fine strontium ferrite particles, while having favorable rheological properties, exhibited undesirable viscoelastic fluid behavior. All the magnetic paste formulations experienced reductions in viscosity with an increase in temperature, yet the formulation modified with the highest amount of rheological additive resulted in a viscosity for low shear rates at the epoxy curing temperature that was over 500 times greater in magnitude compared to the comparable paste without additive. The ability of the material to maintain high viscosity at low shear rates at curing temperatures enabled the control of particle settling, which was validated using XRD and SEM analyses. A rheological additive loading of 10 wt% was observed to be efficient in controlling magnetic particle settling. The developed material formulation enabled the printing of magnetic composites with a filler loading of 50 wt% and 80 wt% using a material jetting based 3D printer. It was observed that the formulations engineered with the additive maintained the printed shape, whereas significant material deformation was observed in unmodified resins. SEM images indicated good distribution and dispersion of magnetic particles within the composite. Magnetic characterization enabled understanding that the resultant magnetic properties are highly dependent on the magnetic powder characteristics, filler loading and the distribution of magnetic particle within the composite. Coercivity was observed to notably decrease with increasing temperature, whereas only a moderate decrease was observed in magnetic remanence. Even through the addition of strontium ferrite enhanced certain rheological characteristics, the magnetic performance was found to be inferior. Overall, this fundamental work yielded thermally stable magnetic material formulations, which enabled the solving of fundamental material and process issues related to additive manufacturing. Future work will include utilizing the developed material formulations to print magnetic composites and characterize cure and mechanical (elastic, fracture) behavior. Additionally, blending processes shall be optimized to reduce porosity and further engineer formulations to reach higher magnetic filler loadings.

Author Contributions: B.N., A.J.Q. and P.M. conceptualized the research framework. B.N. developed formulations, prepared feedstock materials, conducted settling experiments, 3D printed samples, conducted SEM and XRD work, interpreted results and wrote the manuscript. P.M., M.K., S.T., and M.A.W.S. reviewed and revised the manuscript. M.K. conducted rheological tests and M.A.W.S. conducted the magnetic characterization. U.S. and S.T. assisted in providing rheometer and SQUID facilities for the characterization and assisted B.N. in characterizing polymer formulations and magnetic composites. All authors have read and agreed to the published version of the manuscript.

Funding: This work is a part of the University of Alberta's Future Energy Systems research initiative and the Canada First Research Excellence Fund (CFREF). The authors are thankful for the gracious funding to make this research possible. Funding to M.A.W.S. was provided by the Alexander von Humboldt Foundation Feodor Lynen Research Fellowship and the University of Calgary's Global Research Initiative in Sustainable Low Carbon Unconventional Resources funded by the Canada First Research Excellence Fund (CFREF). This research used facilities funded through a grant from the Canadian Foundation for Innovation John R. Evans Leaders Fund (CFI-JELF).

Acknowledgments: The authors would like to express their gratitude to the staff at the nanoFAB and the Department of Earth and Atmospheric Sciences at the University of Alberta for supporting this research and providing access to XRD and SEM facilities.

Conflicts of Interest: The authors declare no conflict of interest.

References

1. Coey, J.M.D. Permanent magnets: Plugging the gap. *Scr. Mater.* **2012**, *67*, 524–529. [CrossRef]
2. Brown, D.; Ma, B.-M.; Chen, Z. Developments in the processing and properties of NdFeb-type permanent magnets. *J. Magn. Magn. Mater.* **2002**, *248*, 432–440. [CrossRef]
3. Ormerod, J.; Constantinides, S. Bonded permanent magnets: Current status and future opportunities (invited). *J. Appl. Phys.* **1997**, *81*, 4816. [CrossRef]
4. Xiao, J.; Otaigbe, J.U. Polymer-bonded magnets: Part I. Analytic thermogravimetry to determine the effect of surface modification on dispersion of Nd–Fe–B fillers. *J. Mater. Res.* **1999**, *14*, 2893–2896. [CrossRef]
5. Najgebauer, M.; Szczygłowski, J.; Ślusarek, B.; Przybylski, M.; Kapłon, A.; Rolek, J. Magnetic Composites in Electric Motors. In *Analysis and Simulation of Electrical and Computer Systems Cham*; Mazur, D., Gołkebiowski, M., Korkosz, M., Eds.; Springer International Publishing: New York, NY, USA, 2018; pp. 15–28.
6. Ertz, G.; Hrynik, T.; Lafleur, D.; Mertiny, P.; Secanell, M.; Wagner, N. Design of Low-Cost Fly Wheel Energy Storage Systems. *SAMPE J.* **2017**, *53*, 18–26.
7. Edwards, L.; Yon, J.; Bond, I.; Mellor, P. Structural Magnetic Composites for Use in Electro-Mechanical Applications. In Proceedings of the ICCM 20th International Conference on Composite Materials, Copenhagen, Denmark, 19–24 July 2015; pp. 1–8.
8. Martin, J.E.; Rohwer, L.E.S.; Stupak, J. Elastic magnetic composites for energy storage flywheels. *Compos. Part B Eng.* **2016**, *97*, 141–149. [CrossRef]
9. Martin, J.; Venturini, E.; Odinek, J.; Anderson, R. Anisotropic magnetism in field-structured composites. *Phys. Rev. E* **2000**, *61*, 2818–2830. [CrossRef]
10. Gibson, I.; Rosen, D.; Stucker, B. *Additive Manufacturing Technologies Additive Manufacturing Technologies: 3D Printing, Rapid Prototyping, and Direct Digital Manufacturing*, 2nd ed.; Springer: New York, NY, USA, 2015; 498p.
11. Mikler, C.V.; Chaudhary, V.; Borkar, T.; Soni, V.; Jaeger, D.; Chen, X.; Contieri, R.; Ramanujan, R.V.; Banerjee, R. Laser Additive Manufacturing of Magnetic Materials. *JOM* **2017**, *69*, 532–543. [CrossRef]
12. Nilsén, F.; Ituarte, I.F.; Salmi, M.; Partanen, J.; Hannula, S.-P. Effect of process parameters on non-modulated Ni-Mn-Ga alloy manufactured using powder bed fusion. *Addit. Manuf.* **2019**, *28*, 464–474. [CrossRef]
13. Yan, Y.; Liu, L.; Ding, C.; Nguyen, L.; Moss, J.; Mei, Y.; Lu, G. Additive manufacturing of magnetic components for heterogeneous integration. In Proceedings of the 2017 IEEE 67th Electronic Components and Technology Conference (ECTC), Orlando, FL, USA, 30 May–2 June 2017; IEEE: Piscataway, NJ, USA, 2017; pp. 324–330.
14. Yan, Y.; Moss, J.; Ngo, K.D.T.; Mei, Y.; Lu, G.-Q. Additive Manufacturing of Toroid Inductor for Power Electronics Applications. *IEEE Trans. Ind. Appl.* **2017**, *53*, 5709–5714. [CrossRef]
15. Compton, B.G.; Kemp, J.W.; Novikov, T.V.; Pack, R.C.; Nlebedim, C.I.; Duty, C.E.; Rios, O.; Paranthaman, M.P. Direct-write 3D printing of NdFeB bonded magnets. *Mater. Manuf. Process.* **2016**, 1–5. [CrossRef]
16. Li, L.; Tirado, A.; Nlebedim, I.C.; Rios, O.; Post, B.; Kunc, V.; Lowden, R.R.; Lara-Curzio, E.; Fredette, R.; Ormerod, J.; et al. Big Area Additive Manufacturing of High Performance Bonded NdFeB Magnets. *Sci. Rep.* **2016**, *6*, 1–7. [CrossRef] [PubMed]
17. Gandha, K.; Li, L.; Nlebedim, I.C.; Post, B.K.; Kunc, V.; Sales, B.C.; Bell, J.; Paranthaman, M.P. Additive manufacturing of anisotropic hybrid NdFeB-SmFeN nylon composite bonded magnets. *J. Magn. Magn. Mater.* **2018**, *467*, 8–13. [CrossRef]
18. Nagarajan, B.; Eufracio Aguilera, A.F.; Wiechmann, M.; Qureshi, A.J.; Mertiny, P. Characterization of magnetic particle alignment in photosensitive polymer resin: A preliminary study for additive manufacturing processes. *Addit. Manuf.* **2018**, *22*, 528–536. [CrossRef]
19. Palmero, E.M.; Casaleiz, D.; Jimenez, N.A.; Rial, J.; de Vicente, J.; Nieto, A.; Altimira, R.; Bollero, A. Magnetic-Polymer Composites for Bonding and 3D Printing of Permanent Magnets. *IEEE Trans. Magn.* **2019**, *55*, 1–4. [CrossRef]

20. Khatri, B.; Lappe, K.; Noetzel, D.; Pursche, K.; Hanemann, T. A 3D-Printable Polymer-Metal Soft-Magnetic Functional Composite—Development and Characterization. *Materials* **2018**, *11*, 189. [CrossRef]
21. von Petersdorff-Campen, K.; Hauswirth, Y.; Carpenter, J.; Hagmann, A.; Boës, S.; Schmid Daners, M.; Penner, D.; Meboldt, M. 3D Printing of Functional Assemblies with Integrated Polymer-Bonded Magnets Demonstrated with a Prototype of a Rotary Blood Pump. *Appl. Sci.* **2018**, *8*, 1275. [CrossRef]
22. Mezger, T.G. The Rheology Handbook. *Pigment Resin Technol.* **2009**, *38*. [CrossRef]
23. *ASTM E3070-18 Standard Test Method for Shear Thinning Index of Non-Newtonian Liquids Using a Rotational Viscometer*; ASTM International: West Conshohocken, PA, USA, 2018; Available online: http://www.astm.org/cgi-bin/resolver.cgi?E3070-18 (accessed on 9 January 2020).
24. Elbadawi, M.; Rivera-Armenta, J.L.; Cruz, B.A.S. Polymeric Additive Manufacturing: The Necessity and Utility of Rheology. In *Polymer Rheology*; IntechOpen: Rijeka, Croatia, 2018; pp. 43–63.
25. Burlawar, S.; Klingenberg, D.J.; Root, T.W.; Schlafmann, K.; Tim Scott, C. Effect of temperature on the rheology of concentrated fiber suspensions. *J. Rheol.* **2019**, *63*, 677–691. [CrossRef]
26. Sotomayor, M.E.; Várez, A.; Levenfeld, B. Influence of powder particle size distribution on rheological properties of 316L powder injection moulding feedstocks. *Powder Technol* **2010**, *200*, 30–36. [CrossRef]
27. Eufracio Aguilera, A.F.; Nagarajan, B.; Fleck, B.A.; Qureshi, A.J. Ferromagnetic particle structuring in material jetting—Manufacturing control system and software development. *Procedia Manuf.* **2019**, *34*, 545–551. [CrossRef]
28. Ranellucci, A. Slic3r. Available online: https://slic3r.org/ (accessed on 27 September 2019).
29. Schneider, C.A.; Rasband, W.S.; Eliceiri, K.W. NIH Image to ImageJ: 25 years of image analysis. *Nat. Methods* **2012**, *9*, 671. [CrossRef] [PubMed]
30. Kamkar, M.; Aliabadian, E.; Shayesteh Zeraati, A.; Sundararaj, U. Application of nonlinear rheology to assess the effect of secondary nanofiller on network structure of hybrid polymer nanocomposites. *Phys. Fluids* **2018**, *30*, 023102. [CrossRef]
31. Manning, K.B.; Wyatt, N.; Hughes, L.; Cook, A.; Giron, N.H.; Martinez, E.; Campbell, C.G.; Celina, M.C. Self Assembly–Assisted Additive Manufacturing: Direct Ink Write 3D Printing of Epoxy–Amine Thermosets. *Macromol. Mater. Eng.* **2019**, *304*, 1800511. [CrossRef]
32. Wang, H.; Liu, X.; Apostolidis, P.; Scarpas, T. Rheological Behavior and Its Chemical Interpretation of Crumb Rubber Modified Asphalt Containing Warm-Mix Additives. *Transp. Res. Rec. J. Transp. Res. Board* **2018**, *2672*, 337–348. [CrossRef]
33. Berndlmaier, R. Rheology additives for coatings. In *Handbook of Coating Additives*; John, J., Florio, D.J.M., Eds.; Marcel Dekker Inc.: New York, NY, USA, 2008; pp. 363–403.
34. Kamkar, M.; Sadeghi, S.; Arjmand, M.; Sundararaj, U. Structural Characterization of CVD Custom-Synthesized Carbon Nanotube/Polymer Nanocomposites in Large-Amplitude Oscillatory Shear (LAOS) Mode: Effect of Dispersion Characteristics in Confined Geometries. *Macromolecules* **2019**, *52*, 1489–1504. [CrossRef]
35. Aliabadian, E.; Sadeghi, S.; Kamkar, M.; Chen, Z.; Sundararaj, U. Rheology of fumed silica nanoparticles/partially hydrolyzed polyacrylamide aqueous solutions under small and large amplitude oscillatory shear deformations. *J. Rheol.* **2018**, *62*, 1197–1216. [CrossRef]
36. Rezvani Moghaddam, A.; Kamkar, M.; Ranjbar, Z.; Sundararaj, U.; Jannesari, A.; Ranjbar, B. Tuning the Network Structure of Graphene/epoxy nanocomposites by Controlling Edge/Basal Localization of Functional Groups. *Ind. Eng. Chem. Res.* **2019**, *58*, 21431–21440. [CrossRef]
37. Nlebedim, I.C.; Ucar, H.; Hatter, C.B.; McCallum, R.W.; McCall, S.K.; Kramer, M.J. Studies on in situ magnetic alignment of bonded anisotropic Nd-Fe-B alloy powders. *J. Magn. Magn. Mater.* **2017**, *422*, 168–173. [CrossRef]
38. Su, K.P.; Liu, Z.W.; Zeng, D.C.; Huo, D.X.; Li, L.W.; Zhang, G.Q. Structure and size-dependent properties of NdFeB nanoparticles and textured nano-flakes prepared from nanocrystalline ribbons. *J. Phys. D Appl. Phys.* **2013**, *46*, 245003. [CrossRef]
39. Wang, X.F.; Lee, D.; Jiang, Z.L. Magnetic properties of hybrid polymer bonded Nd–Fe–B/ferrite magnets. *J. Appl. Phys.* **2006**, *99*, 08B513. [CrossRef]